Resting state changes in aging and Parkinson's disease are shaped by underlying neurotransmission – a normative modeling study

Jan Kasper[1,2], Svenja Caspers[3,4], Leon D. Lotter[1,2,5], Felix Hoffstaedter[1,2], Simon B. Eickhoff[1,2], Juergen Dukart[1,2,*]

[1]Institute of Systems Neuroscience, Medical Faculty & University Hospital Düsseldorf, Heinrich Heine University Düsseldorf, Düsseldorf, Germany
[2]Institute of Neuroscience and Medicine (INM-7), Research Centre Jülich, Jülich, Germany
[3]Institute of Neuroscience and Medicine (INM-1), Research Centre Jülich, Jülich, Germany
[4]Institute for Anatomy I, Medical Faculty & University Hospital Düsseldorf, Heinrich Heine University Düsseldorf, Düsseldorf, Germany
[5]Max Planck School of Cognition, Stephanstrasse 1A, 04103 Leipzig, Germany

*Corresponding author:

Juergen Dukart, PhD

Institute of Neuroscience and Medicine - INM-7: Brain and Behaviour, Research Center Jülich

Institute of Systems Neuroscience, Medical Faculty, Heinrich Heine University Düsseldorf

Wilhelm-Johnen-Straße,

52425 Jülich, Germany

Email: juergen.dukart@gmail.com

Abstract

Human healthy and pathological aging is linked to a steady decline in brain resting state activity and connectivity measures. The neurophysiological mechanisms underlying these changes remain poorly understood. Making use of recent developments in normative modeling and availability of in vivo maps for various neurochemical systems, we test in the UK Biobank cohort (N=25,917) if and how age- and Parkinson's disease related resting state changes in commonly applied local and global activity and connectivity measures co-localize with underlying neurotransmitter systems. We find the distributions of several major neurotransmitter systems including serotonergic, dopaminergic, noradrenergic and glutamatergic neurotransmission to explain age-related changes as observed across functional activity and connectivity measures. Co-localization patterns in Parkinson's disease deviate from normative aging trajectories for these, as well as for cholinergic and GABAergic neurotransmission. The deviation from normal co-localization of brain function and GABAa correlates with disease duration. These findings provide new insights into molecular mechanisms underlying age- and Parkinson's related brain functional changes. Combining normative modeling and neurotransmitter mapping may aid future research and drug development through deeper understanding of neurophysiological mechanisms underlying specific clinical conditions.

Abbreviations: rs-fMRI: Resting-state functional magnet resonance imaging; PD: Parkinson's disease; SERT: Serotonin transporter; DAT: Dopamine transporter; VAChT: Vesicular acetylcholine transporter; NET: Norepinephrine transporter; PET: Positron emission tomography; BOLD: blood oxygenation level dependent; fALFF: Fractional amplitude of low-frequency fluctuations; LCOR: Local correlation; GCOR: Global correlation; FWHM: Full width at half maximum; HC: Healthy controls; TIV: total intracranial volume; SD: Standard deviation; BH: Bonferroni-Holm; FDR: False discovery rate

Introduction

Understanding the neurophysiological mechanisms underlying healthy and pathological brain aging is an essential component for development of successful prevention, detection, and intervention strategies for age-related diseases and cognitive decline. Despite ample evidence for age-related decline in various brain functional measures there is only limited understanding of the neurophysiological mechanisms underlying these changes. As the interplay of different neurotransmitter systems is the major contributor to the blood oxygen level dependent (BOLD) signal it is plausible to assume that changes in respective systems also manifest in age-related functional alterations as observed using resting state functional magnetic resonance imaging (rs-fMRI).

Most commonly applied rs-fMRI measures estimate either the temporal change in the regional amplitude of the BOLD signal as a measure of local activity, or compute correlations of BOLD time series across different brain regions as a measure of synchronicity. Previous rs-fMRI studies reported aging related reductions in local brain activity primarily in medial and frontal regions[1–4]. These alterations are complemented by reduced local synchronicity in cortical, sub-cortical, and cerebellar motor structures[5] and increased local synchronicity mainly in hippocampal and thalamic regions[4,6]. In parallel, positron emission tomography (PET) studies of aging reported reduced serotonergic[7–11], dopaminergic[12–15], glutamatergic[16–18], cholinergic[19] and norepinephrinergic[20] neurotransmission whilst evidence for increased availability was found for GABAa[21] and μ-opioid[22] receptors. Whilst both modalities point to complex functional re-organization during aging, the relationship between the respective rs-fMRI and PET findings remains poorly understood.

Testing for associations between the regional availability of specific neurotransmitter receptors or transporters as derived from positron emission tomography (PET) and rs-fMRI derived functional signal has been shown to be a promising way to estimate their impact on the observed brain phenotypes[23,24]. To date, age-related changes in these associations have not been systematically addressed. Such age-related changes in co-localization patterns may reflect the altered availability or functional decline of cell populations that exhibit the respective neurochemical properties. Following this logic, disease related changes in such associations would support the notion of respective neurotransmitter systems being particularly affected by the respective neuropathology[25].

Understanding of typical age-related co-localization changes of brain function and neurotransmitter systems can inform the study of pathological deviations from such as for example observed in Parkinson's disease[25] (PD). Previous studies provided evidence for increased vulnerability of specific neurotransmitter systems in PD including dopaminergic[26–31], serotonergic[32–34], glutamatergic[35,36], GABAergic[30], histaminergic[37], cholinergic[38–40], and norepinphrinergic[41,42] neurotransmission. In our previous work, deviations from normal brain function in PD were related to the availability of D2 and 5-HT1b receptors, supporting the notion of specific vulnerability of these neurotransmitter systems[25]. However, if and how far these PD-related alterations deviate from typical age-related co-localization changes remains to be shown.

To address these questions, we adopt a normative modeling approach to test for aging-effects on co-localizations between brain resting state functional measures and underlying neurotransmission in a large cohort drawn from the UK Biobank (n = 25,917). We then replicate and extend the previous evidence of increased vulnerability of specific neurotransmitter systems in PD (n = 58). We test for co-localization of PET-derived distributions for all major neurotransmitter systems with commonly deployed rs-fMRI derived activity and connectivity measures.

Methods

Cohorts

We included 25,917 adult subjects from the UK Biobank who were not diagnosed with any of the listed diseases (Supplementary Table 1) as a control cohort for normative modeling of aging effects. Subjects with psychiatric, cognitive, and neurological disorders with known effect on brain structure (like demyelinating diseases or atrophies) and function (like intellectual disabilities, psychoactive substance use, or schizophrenia) were excluded. We additionally identified a group of 58 subjects from the UK Biobank who were diagnosed with idiopathic Parkinson's disease (ICD-10, G20) before their imaging session. An overview of both groups is provided in Table 1.

Preprocessing of resting-state functional imaging data

We used resting-state functional MRI data provided and processed by the UK Biobank (referred to as "filtered_func_data_clean.nii", cf. UK Biobank Brain Imaging Documentation for a detailed description[43]). The pipeline consisted of primary T1 quality control, gradient distortion correction, motion correction, grand-mean intensity normalization, high-pass temporal filtering, echo planar imaging unwarping, gradient distortion correction unwarping, and the removal of structural artefacts via ICA+FIX. Further processing was conducted with SPM12[44], the FMIRB Software Library (FSL v5.0[45]), and the CONN toolbox[46] implemented in MATLAB (v2020b). Functional images were transformed into MNI space using a general reference template provided by FSL and a subject specific warping image. After resampling (3mm^3 isotropic) and smoothing (Gaussian kernel with 4 mm FWHM), we applied a bandpass filter (0.008 – 0.09 Hz) to the BOLD signal, discarded the first five frames to ensure signal equilibrium, and regressed out 24 parameters of motion[47], as well as the mean signal from white matter and cerebrospinal fluid. Distorted images and artifacts were identified by low correlations ($r < 0.9$) between individual and a reference, preprocessed mean rs-fMRI image of 200 subjects. Visual inspection confirmed that failed spatial normalization or insufficient brain coverage in individual images were responsible for low correlation coefficients. We additionally excluded data from subjects with excessive in-scanner motion (maximum frame-wise rotation $> 2°$ and movement > 3 mm).

Measures of local brain activity and synchronicity

Three complementary maps of brain function, including measures of neuronal activity and synchronicity were derived from individual, preprocessed rs-fMRI data using the CONN toolbox. As a proxy for spontaneous local neuronal activity, we calculated voxel-wise maps of the fractional amplitude of low-frequency fluctuations (fALFF). fALFF is defined as the power ratio of low-frequency (0.008 – 0.09 Hz) oscillations to the total detectable frequency range in the BOLD signal[48]. Maps of local and global correlation (LCOR[49] and GCOR[50]) represent proxies for both BOLD activity and synchronicity. LCOR is defined as the normalized sum of correlation coefficients of the BOLD signal in the voxel of interest with other voxels in its vicinity, with distances weighted by a Gaussian kernel (25 mm FWHM). GCOR is calculated in the same way as LCOR, but without distance-dependent weighting of the individual correlation coefficients. Thus, GCOR represents a measure of the global synchronicity of a

voxel, whereas LCOR represents a measure of local coherence. Unlike fALFF, LCOR and GCOR do not depend on the amplitude of the BOLD signal, but rather on the similarity of the BOLD time series of all considered voxels. These three metrics provide a complementary characterization of the BOLD signal providing information about local neural activity as well as local and global functional connectivity.

Aging effects and sex differences in fALFF, LCOR, and GCOR

We estimated voxel-wise aging effects by general linear modeling of (t-)contrast maps using a family-wise-error corrected voxel-wise threshold of $P < 0.05$ combined with a cluster-defining threshold of $k > 20$, including sex as a covariate. Using voxel-wise beta weights of the aging effects, we generated maps of annual changes in fALFF, LCOR and GCOR. Additionally, we assessed voxel-wise sex effects in fALFF, LCOR, and GCOR between women and men by general linear modeling of (t-)contrast maps using SPM12, including age and total intracranial volume (TIV) as covariates (thresholding as above).

Spatial co-localization of brain function and neurotransmitter systems and effects of aging in the healthy population

We analyzed to what extent unthresholded group-level aging effects (maps of annual change) in fALFF, LCOR, and GCOR co-localize with specific neurotransmitter systems. For this, Spearman correlation coefficients were derived using the default Neuromorphometrics atlas (119 regions) estimating the similarity of aging effects in fALFF, LCOR, and GCOR with 19 distinct neurotransmitter maps as included in the JuSpace toolbox[25]. To approximate a normal distribution, correlation coefficients were Fisher's z-transformed. We choose the Neuromorphometrics atlas as it provides a neuroanatomically plausible delineation of cortical and subcortical structures. As shown in our previous study[51], the choice of atlas (with a comparable number of parcels) has a neglectable effect on the observed co-localization patterns of brain dysfunction and PET maps.

Included PET maps covered serotonergic receptors (5-HT1a[52], 5-HT1b[53], 5-HT2a[52], 5-HT4[52], 5-HT6[11]), dopaminergic receptors (D1[54], D2[55]), histamine receptor 3 (H3[56]), dopamine uptake (DAT[24]), serotonin (SERT[52]), norepinephrine (NET[20]), vesicular acetylcholine (VAChT[57])

transporters, as well as the acetylcholinergic receptors M1[58] and A4B2[59], the glutamate receptors mGluR5[60] and NMDA[61], the cannabinoid CB1[62], opioid μ[57], and the GABAa[24] receptor. Source publications, age, sex, and sample sizes characteristics of each PET map are provided in Supplementary Table 2. 95% confidence intervals of Spearman correlation coefficients were estimated using the Bonett-Wright[63] procedure.

To better understand if and how these group level aging effects are also reflected in terms of the magnitude and the spread across all individual data, we re-computed the correlations on the single-subject level using individual measures of fALFF, LCOR, and GCOR. Prior to testing for aging effects across individual co-localizations, we examined whether Fisher's z-transformed Spearman correlation coefficients of the healthy population were significantly different from a null distribution (one-sample t-test, alpha = 0.05). Aging effects on co-localization strengths were then estimated using linear regression analyses considering sex as a confound.

Higher variation in co-localization between brain function and neurotransmitter systems with aging

Distinct aging trajectories from healthy aging to the effects of diseases and impairments are known to manifest in altered brain function. Depending on the underlying neurophysiological processes such changes are likely to be architecturally aligned with the spatial patterns of affected neurotransmitter systems. Correspondingly, one would expect to observe an increased variation in co-localization between brain function and receptor/transporter distribution in older as compared to younger participants. To test this hypothesis, we examined the heteroscedasticity in co-localization to identify neurotransmitter systems that are affected by such age-related brain functional changes.

For this, we performed two complementary tests. Using the White test, we first identified all pairs of brain function measures and PET maps whose correlation coefficients did not exhibit constant variance across age. In a post-hoc analysis, we tested for each co-localization pair with non-constant variance ($P_{FDR} < 0.05$) whether the variance for individuals in the upper third age-range is higher as compared to those in the lower third age-range using the Goldfeld-Quandt-test (one-sided, i.e., increasing variance). To account for potential confounding effects of sex

between younger and older adults, we regressed out sex effects from the Fisher's z-transformed Spearman correlation coefficients prior to the comparisons.

Normative modeling of brain function - neurotransmitter co-localization and deviations in Parkinson's disease

To model the effects of aging on the observed co-localization patterns we generated normative models based on the Fisher's transformed correlation coefficients (co-localization strengths between neurotransmitter and rs-fMRI measures) derived from the healthy UK Biobank subjects using the PCNtoolkit[64]. To account for non-linear trajectories and non-Gaussian variance of the normal co-localization levels, we used Bayesian linear regression (5 knot basis splines and sinh-arcsinh warping) with age and sex as covariates (cf. Figure 1 for a methodological overview).

Deviations (z-scores) from these normative aging models were derived per neurotransmitter map for subjects with PD. By comparing the deviation scores to a null distribution (t-test, alpha = 0.05), we identified neurotransmitter co-localization pairs for which patients with PD differed from normative models derived from healthy controls. For the significant ($P_{FDR} < 0.05$) deviations, we tested which regions contributed strongest to the observed deviations. To this end, we repeated the spatial correlation analyses in the data of PD using a leave-one-region-out approach[65]. As a measure of regional contribution to the deviation we calculated differences in squared correlation coefficients ($\Delta\rho^2$) between the reduced ($n_{Regions} = 118$: ρ_{LOO}^2) and the full ($n_{Regions} = 119$: ρ_{Total}^2) set of regions. We set $\Delta\rho^2$ positive if omitting this specific region resulted in a more normal correlation coefficient (closer to the mean of the normative model), and negative if omitting led to stronger deviation from the normative model. We further evaluated whether these regional contributions to the observed co-localization strengths were spatially related to regional alterations in fALFF, LCOR, or GCOR by computing Pearson correlations between maps of $\Delta\rho^2$ and the regional effect size (Cohen's d) in fALFF, LCOR, GCOR for differences between PD and an age- and sex-matched subgroup of HC (n = 17,400). In order to evaluate the extent of significant functional alterations in PD, regions with significant differences in fALFF, LCOR, and GCOR in PD compared with the matched controls were identified using the Mann-Whitney-U test.

All analyses were corrected for multiple comparisons using either the Benjamini-Hochberg procedure or, in case of highly inflated P-values due to large sample sizes, Bonferroni-Holm

correction. To ensure that the observed functional co-localization effects are not driven by the underlying atrophy we repeated all analyses after regressing out the individual voxel-wise grey matter volumes (spatially smoothed with a 4 mm FWHM Gaussian kernel) from all functional maps.

Results

Demographic characterization

From a total pool of 30,035 subjects from the UK Biobank for which all necessary functional images and movement data was available, our analysis was based on data of 25,917 subjects for whom no diseases with known effect on brain function were reported.

Three subjects had no structural data available. Thus, the repetition of all analysis after controlling for age-related atrophy was performed on the data of 25,914 subjects. 75 subjects of the total pool had reported a diagnosis of Parkinson's disease. In 58 of them, the first mention of the diagnosis (ICD-10: G20) was dated before their imaging session, so we classified them as "manifest" and included them for further analysis. In order to compare regional measures of brain function in PD with those of the healthy controls, we defined an age- and sex-matched subcohort consisting of 17,400 subjects (PD mean $\pm$ SD age in years: 68.6 ± 6.5, $HC_{matched}$ mean $\pm$ SD age: 67.6 ± 6.0, P>0.26; 55.17% male PD and 51.7% male $HC_{matched}$, $\chi^2(1)=0.29$, P=0.59). An overview of the groups is provided in Table 1.

Group-level aging effects in resting state measures and their co-localization to underlying neurotransmission

All three resting state measures decreased with aging in most cortical, sub-cortical, and cerebellar regions. Each measure showed a wide-spread but distinct spatial pattern of age-related alterations with few regional increases (Figure 2A, Supplementary Table 3 and Supplementary Table 4).

Next, we aimed to understand if the topography of these age-related changes was linked to the distribution of specific neurotransmitter systems. For this, we derived voxel-wise maps of age-related linear (annual) changes in all three resting state measures and tested for their spatial co-localization with the neurotransmitter systems. The rate at which fALFF and LCOR changed during aging correlated significantly ($P_{FDR}<0.05$) with serotonergic, dopaminergic, norepinephrinergic (also GCOR) and glutamate neurotransmission (Figure 2B, Supplementary Figures 1-2, Supplementary Tables 5-6). In addition, fALFF changes correlated with GABAergic and LCOR changes with cholinergic neurotransmission. Except for the correlation between fALFF changes and NMDA all findings remained significant after correcting for age-related atrophy. Scatter plots of the strongest correlations are displayed in Figure 2B. Results for voxel-wise sex differences are summarized in Supplementary Figures 3-5 and Supplementary Tables 7-10.

Individual co-localization of resting state measures and neurotransmitter systems covaries with age

The extent to which a specific neurotransmitter system contributes to the measured brain function was evaluated by its correlation strength. We first computed the individual co-localization strengths between each subject's resting state measure and each available neurotransmitter map. Due to the large cohort size, even very small effects in all resting state measures were significantly associated with the 19 PET maps (all $P_{Bonferroni-Holm}<0.0001$, median absolute Spearman correlation coefficient ranged from 0.03 to 0.68) with the different neurotransmitter systems explaining between 0.1% and 46% of variance in the respective resting state measures (Supplementary Figure 6, Supplementary Tables 11-13, left columns). The direction of the correlations was highly similar across the three functional measures. Positive correlations were found for the norepinephrinergic, muscarinic, glutamatergic, GABAergic systems, as well as serotonergic receptors 5-HT1b, -2a, and -6. Negative correlations were found for the dopaminergic, histaminergic and opioid neurotransmitter systems, as well as for serotonin receptors 5-HT1a, 5-HT4 and serotonin and vesicular acetylcholine transporters (SERT and VAChT). All associations remained significant after controlling for age-related atrophy (Supplementary Tables 14-16). If age-related changes in brain functions are indeed primarily driven by specific neurotransmitter systems, the correlation coefficients should systematically (that is, in simplest approximation, linearly) in- or decrease

during aging. Thus, we tested whether and to what extent aging effects and their co-localizations with neurotransmitter systems observed at the cohort level are also reflected in the individual co-localization strength. Most of the observed correlations were significantly associated with age explaining up to 3%, 4% and 1% of the co-localization strength between fALFF (with NMDA and SERT), LCOR (with SERT) and GCOR (with VAChT) and the respective neurotransmitter systems (Figure 3A, Supplementary Tables 11-13, middle columns). Correction for atrophy lowered the correlation strengths for most associations but the findings remained largely significant (Supplementary Tables 14-16, middle columns).

Variance in co-localization changes during aging

As aging may not only be associated with changes in average co-localization strengths but also with increased variance in such (i.e., due to yet undetected neurodegenerative processes in a subpopulation) we tested for such changes using a two-step procedure. Using the White-test, we first identified significant non-constant variance in co-localization strength. For fALFF and LCOR, non-constant variance was observed for all classes of neurotransmitters except for LCOR and opioid system. For GCOR, significant non-constant variance in co-localization was found for serotoninergic, norepinephrinergic, cannabinoid, opioid, glutamatergic and cholinergic neurotransmission (Supplementary Table 17, left columns). These effects remained significant after controlling for age-related atrophy except for GCOR and 5-HT1b, 5-HT6, and SERT (Supplementary Table 18, left columns). As the above analysis only detects differences in variance over age but not their direction, we aimed to better understand the respective findings by computing the Goldfeld-Quandt test comparing the co-localization variance between the youngest (44 – 60 years) and oldest (68 – 82 years) third (n_{Both} =8,639) of the study population for the significant associations identified using the White-test (Figure 3B).

For fALFF and LCOR, higher variability in co-localization was found in the elderly sub-population for serotonergic, dopaminergic, noradrenergic, histaminergic, cannabinoid, glutamatergic and cholinergic neurotransmission. In addition, for LCOR, we found significantly higher variance in the older population in co-localization with the GABA system. For GCOR, higher variability in co-localization was found regarding the serotonergic, noradrenergic, glutamatergic, and cholinergic system. For fALFF, 11 out of 14, for LCOR, 14 out of 15 and for GCOR, 7 out of 11 neurotransmitter co-localization pairs identified using the White-test displayed a higher variance in the older subpopulation (Figure 3B, Supplementary

Table 17, right columns). The effects remained largely similar after controlling for atrophy (Supplementary Table 18, right columns).

Deviations from normal co-localization in manifest Parkinson's disease

Having established this reference for co-localization of normal age-related changes with different neurotransmitter systems, we now aimed to test if and how functional changes caused by progressive neurodegeneration deviate from the non-pathological co-localization patterns. For this, we adopted a normative modeling approach using the healthy aging population as a reference allowing for non-linear changes with age (models are visualized in Supplementary Figures 7-8). A UK Biobank subgroup of PD patients served as an example for the clinical relevance of our findings. For each PD patient, we derived individual deviation (z-)scores quantifying their deviation from the normative model. For fALFF, PD patients had a lower co-localization strength with serotonergic, GABAergic, muscarinic and glutamatergic neurotransmission (Figure 4D). For LCOR and GCOR, PD showed lower co-localizations with serotonergic, dopaminergic, GABAergic, histaminergic, norepinephrinergic, glutamatergic and cholinergic neurotransmitter systems (Figure 4E-F, Supplementary Table 19). The deviation in co-localization strength regarding LCOR and GABAa (illustrated in Figure 4A-B) correlated negatively with disease duration with higher deviations being indicative of longer disease duration (Pearson r = -0.38, P_{FDR} = 0.027; Figure 4C, Supplementary Tables 21-22). After atrophy correction, all deviations remained significant except for the LCOR-5-HT1b and LCOR-VAChT associations (Supplementary Table 20).

Lastly, we aimed to understand which regions contribute most to the observed co-localization alterations in PD. For this, we first analyzed how leaving out each region of the deployed atlas changed the observed correlations. For fALFF, main contributing regions to co-localization changes in PD were the basal ganglia, insula and occipital regions. For LCOR and GCOR, main contributing regions to co-localization changes in PD were the basal ganglia, subcallosal areas, thalamus (LCOR only), basal forebrain, as well as pre- and postcentral, insula and occipital regions (Supplementary Figures 9-11). The effects remained largely similar after controlling for atrophy (Supplementary Figures 12-14). Regional contribution to the deviations found regarding the glutamatergic system significantly correlated with regional alteration in PD in both synchronicity measures (P_{FDR}<0.05, Supplementary Figures 15-16, Supplementary Tables

23-24). Effect sizes in regions that exhibit significant ($P_{FDR}<0.05$) differences in LCOR and GCOR in PD compared to the age- and sex-matched subgroup of HC are provided in Figure 4G-H. Statistics of regional comparison of fALFF, LCOR, and GCOR in PD compared to the matched control group are provided in Supplementary Table 25-26. All regional effect sizes in fALFF, LCOR, and GCOR between PD and the age- and sex-matched subgroup of HC are shown in Supplementary Figures 17-19.

Discussion

Here, we tested how age-related changes in commonly applied resting activity and connectivity measures co-localize with underlying neurotransmission. Consistent with previous studies of aging effects on brain function, we find widespread age-related decreases but also few increases in the three evaluated measures[2,3,66]. These age-related changes display a robust co-localization pattern with various major neurotransmitter systems, including monoamines, glutamate, choline, and GABA, at group- and single-subject level. Variance in the co-localization patterns of these systems increases over age. PD patients display significant deviations from typical age-related co-localization patterns in neurotransmitter systems related to the disease. The deviation in co-localization strength regarding the GABAergic system correlates with disease duration.

In line with most studies reporting aging effects in the brain, we find wide-spread age-related decreases in all three evaluated resting state measures[1-5]. The extent of the decreases is substantially higher in our study covering basically all of the brain with few exceptions as discussed below. Considering that these findings are based on over 25,000 subjects, the increased statistical power as compared to previous studies with at most few hundred participants is the most likely explanation for the observed discrepancy. In parallel, we observe spatially distinct age-related increases across the three evaluated resting state measures covering parietal, precuneal, thalamic, gyrus rectus and cerebellar regions. With respect to directionality, these findings are consistent with several previous studies, reporting presumably compensation-related increases in different connectivity metrics in the aging population[66,67]. Consistent with this interpretation, we find the local activity and connectivity to be increased in parietal regions involved in cross-modal sensory integration, potentially compensating for the prominent loss in modality-specific sensory processing during aging[68,69].

Supporting the previously reported complex re-organization of the excitation/inhibition balance during aging[70], we find the group-level aging effects on brain function to be associated with glutamatergic and GABAergic neurotransmission. The additional co-localization of the aging effects with monoaminergic and cholinergic systems may be supportive of the underlying changes to be related to learning, memory, and other higher cognitive functions affected by aging[7,15,67,71]. In contrast, the age-related global connectivity is primarily increased in thalamic and cerebellar regions and the topography of these changes only aligns with the norepinephrinergic neurotransmission. Both regions and in particular the thalamus show a high expression of norepinephrine receptors[72,73]. Whilst the modulatory role of norepinephrine in the cerebellum has been repeatedly associated with motor learning[74,75], its contribution to aging is controversially discussed with its activity being associated with prevention but also acceleration of the production and accumulation of amyloid-β and tau across the brain[76]. On a functional level, these findings may originate in the functional decline of the norepinephrinergic system, which is considered as key factor in maintaining arousal and cognitive adaptation and control[77,78].

When testing for co-localization of resting state measures with neurotransmission at the single subject level, we find age-related alterations in all three measures to co-localize primarily with monoaminergic neurotransmission. These findings are complemented by increases in variance observed for a variety of evaluated neurotransmitter systems. Considering the reportedly high prevalence of neuropathology in a cognitively normal elderly population[79,80] the individual co-localization changes - aside with increased variance - may indeed reflect such yet undetected neurodegenerative processes. To test the sensitivity of the co-localization patterns to such neurodegenerative processes we further adopted a normative modeling approach. A major advantage of normative models is their ability to represent population heterogeneity in the phenotype under investigation by means of normalized deviation scores[64]. We applied this approach in patients with a diagnosis of Parkinson's disease, which was previously linked to monoaminergic neurotransmission as well as more recently to a dysbalance of GABA and glutamate[81–83]. Indeed, across all three resting state metrics we find the co-localization patterns in PD patients to significantly deviate from age- and sex-adjusted normative models across a variety of neurotransmitter systems. Deviations in co-localization of local activity in PD are found primarily with respect to serotonergic, GABA, and glutamatergic neurotransmission, whilst deviations in co-localization of both local and global connectivity are also present with respect to dopamine neurotransmission. We find that only the deviation in co-localization

strength of local connectivity with GABAa receptors predicts disease duration supporting the suggested relevance of GABA pathology for clinical progression[81].

It is important to acknowledge that the studied cohort was recruited as a representative sample of healthy residents of the UK. Because the metrics we studied target local brain function, subjects with diseases primarily affecting brain structure or function were excluded. Given the prevalence for mild depressive symptoms of the UK population of 11 %[84] and that 12.32 % of our analyzed participants of the UK Biobank have a reference to ICD-10: F32, their exclusion would have biased the cohort. Additional healthy control biases in the UK biobank[85] include a high average socioeconomic status, low alcohol and tobacco consume. Although, we estimate that deviations from the overall population results are small with respect to these primary biases, further sampling of a more diverse population is needed for replication. In addition, clinical scores superior to disease duration as an estimate of disease severity should be used to strengthen evidence of the observed association with GABAergic neurotransmission. The use of PET maps from differently aged healthy populations may introduce a further bias into our findings as proteomics such as receptor and transporter distributions may change during aging[77,86].

Conclusions

Here, we provided a detailed overview on the effects of aging on macroscopic brain functioning as observed using rs-fMRI derived commonly measures of local activity and local and global connectivity. We link these age-related changes to the distribution of various major neurotransmitter systems demonstrating a decline in co-localization strength aside with increased variance during aging. By adopting a normative modeling approach, we further demonstrate on the example of Parkinson's disease the feasibility of using co-localization strength as a sensitive measure of underlying neurodegeneration providing potentially valuable insight into the underlying neuropathological processes.

References

1. Biswal BB, Mennes M, Zuo XN, et al. Toward discovery science of human brain function. *Proc Natl Acad Sci USA*. 2010;107(10):4734-4739. doi:10.1073/pnas.0911855107

2. Hu S, Chao HHA, Zhang S, Ide JS, Li CSR. Changes in cerebral morphometry and amplitude of low-frequency fluctuations of BOLD signals during healthy aging: correlation with inhibitory control. *Brain Struct Funct*. 2014;219(3):983-994. doi:10.1007/s00429-013-0548-0

3. Vieira BH, Rondinoni C, Garrido Salmon CE. Evidence of regional associations between age-related inter-individual differences in resting-state functional connectivity and cortical thinning revealed through a multi-level analysis. *NeuroImage*. 2020;211:116662. doi:10.1016/j.neuroimage.2020.116662

4. Montalà-Flaquer M, Cañete-Massé C, Vaqué-Alcázar L, Bartrés-Faz D, Peró-Cebollero M, Guàrdia-Olmos J. Spontaneous brain activity in healthy aging: An overview through fluctuations and regional homogeneity. *Front Aging Neurosci*. 2023;14:1002811. doi:10.3389/fnagi.2022.1002811

5. Wu T, Zang Y, Wang L, Long X, Li K, Chan P. Normal aging decreases regional homogeneity of the motor areas in the resting state. *Neuroscience Letters*. 2007;423(3):189-193. doi:10.1016/j.neulet.2007.06.057

6. Harrison TM, Maass A, Adams JN, Du R, Baker SL, Jagust WJ. Tau deposition is associated with functional isolation of the hippocampus in aging. *Nat Commun*. 2019;10(1):4900. doi:10.1038/s41467-019-12921-z

7. Karrer TM, McLaughlin CL, Guaglianone CP, Samanez-Larkin GR. Reduced serotonin receptors and transporters in normal aging adults: a meta-analysis of PET and SPECT imaging studies. *Neurobiology of Aging*. 2019;80:1-10. doi:10.1016/j.neurobiolaging.2019.03.021

8. Sheline YI, Mintun MA, Moerlein SM, Snyder AZ. Greater Loss of 5-HT $_{2A}$ Receptors in Midlife Than in Late Life. *AJP*. 2002;159(3):430-435. doi:10.1176/appi.ajp.159.3.430

9. Nord M, Cselenyi Z, Forsberg A, et al. Distinct regional age effects on [^{11}C]AZ10419369 binding to 5-HT 1B receptors in the human brain. *NeuroImage*. 2014;103:303-308. doi:10.1016/j.neuroimage.2014.09.040

10. Madsen K, Haahr MT, Marner L, et al. Age and sex effects on 5-HT $_4$ receptors in the human brain: A [^{11}C]SB207145 PET study. *J Cereb Blood Flow Metab*. 2011;31(6):1475-1481. doi:10.1038/jcbfm.2011.11

11. Radhakrishnan R, Nabulsi N, Gaiser E, et al. Age-Related Change in 5-HT $_6$ Receptor Availability in Healthy Male Volunteers Measured with ^{11}C-GSK215083 PET. *J Nucl Med*. 2018;59(9):1445-1450. doi:10.2967/jnumed.117.206516

12. Antonini A, Leenders KL, Reist H, Thomann R, Beer HF, Locher J. Effect of Age on D2 Dopamine Receptors in Normal Human Brain Measured by Positron Emission Tomography and 11C-Raclopride. *Archives of Neurology*. 1993;50(5):474-480. doi:10.1001/archneur.1993.00540050026010

13. Seaman KL, Smith CT, Juarez EJ, et al. Differential regional decline in dopamine receptor availability across adulthood: Linear and nonlinear effects of age. *Hum Brain Mapp*. Published online April 2019:hbm.24585. doi:10.1002/hbm.24585

14. Wang Y, Chan GLY, Holden JE, et al. Age-dependent decline of dopamine D1 receptors in human brain: A PET study. *Synapse*. 1998;30(1):56-61. doi:10.1002/(SICI)1098-2396(199809)30:1<56::AID-SYN7>3.0.CO;2-J

15. Karrer TM, Josef AK, Mata R, Morris ED, Samanez-Larkin GR. Reduced dopamine receptors and transporters but not synthesis capacity in normal aging adults: a meta-analysis. *Neurobiology of Aging*. 2017;57:36-46. doi:10.1016/j.neurobiolaging.2017.05.006

16. Magnusson. Selective vulnerabilities of N-methyl-D-aspartate (NMDA) receptors during brain aging. *FrontiAgNeurosci*. Published online 2010. doi:10.3389/fnagi.2010.00011

17. Perry EK, Piggott MA, Court JA, Johnson M, Perry RH. Transmitters in the Developing and Senescent Human Brain. *Annals of the New York Academy of Sciences*. 1993;695(1):69-72. doi:10.1111/j.1749-6632.1993.tb23030.x

18. Piggott MA, Perry EK, Perry RH, Court JA. [3H]MK-801 binding to the NMDA receptor complex, and its modulation in human frontal cortex during development and aging. *Brain Research*. 1992;588(2):277-286. doi:10.1016/0006-8993(92)91586-4

19. Zubieta JK, Koeppe RA, Frey KA, et al. Assessment of muscarinic receptor concentrations in aging and Alzheimer disease with [11C]NMPB and PET. *Synapse*. 2001;39(4):275-287. doi:10.1002/1098-2396(20010315)39:4<275::AID-SYN1010>3.0.CO;2-3

20. Ding YS, Singhal T, Planeta-Wilson B, et al. PET imaging of the effects of age and cocaine on the norepinephrine transporter in the human brain using (S,S)-[^{11} C]O-methylreboxetine and HRRT. *Synapse*. 2010;64(1):30-38. doi:10.1002/syn.20696

21. Cuypers K, Hehl M, Van Aalst J, et al. Age-related GABAergic differences in the primary sensorimotor cortex: A multimodal approach combining PET, MRS and TMS. *NeuroImage*. 2021;226:117536. doi:10.1016/j.neuroimage.2020.117536

22. Zubieta JK, Dannals RF, Frost JJ. Gender and Age Influences on Human Brain Mu-Opioid Receptor Binding Measured by PET. *AJP*. 1999;156(6):842-848. doi:10.1176/ajp.156.6.842

23. Hansen JY, Shafiei G, Markello RD, et al. Mapping neurotransmitter systems to the structural and functional organization of the human neocortex. *Nat Neurosci*. 2022;25(11):1569-1581. doi:10.1038/s41593-022-01186-3

24. Dukart J, Holiga Š, Chatham C, et al. Cerebral blood flow predicts differential neurotransmitter activity. *Sci Rep*. 2018;8(1):4074. doi:10.1038/s41598-018-22444-0

25. Dukart J, Holiga S, Rullmann M, et al. JuSpace: A tool for spatial correlation analyses of magnetic resonance imaging data with nuclear imaging derived neurotransmitter maps. *Hum Brain Mapp*. 2021;42(3):555-566. doi:10.1002/hbm.25244

26. Kaasinen V, Vahlberg T, Stoessl AJ, Strafella AP, Antonini A. Dopamine Receptors in Parkinson's Disease: A Meta-Analysis of Imaging Studies. *Mov Disord*. 2021;36(8):1781-1791. doi:10.1002/mds.28632

27. Kaasinen V, Nagren K, Hietala J, et al. Extrastriatal dopamine D2 and D3 receptors in early and advanced Parkinson's disease. *Neurology*. 2000;54(7):1482-1487. doi:10.1212/WNL.54.7.1482

28. Seeman P, Niznik HB. Dopamine receptors and transporters in Parkinson's disease and schizophrenia. *FASEB j*. 1990;4(10):2737-2744. doi:10.1096/fasebj.4.10.2197154

29. Politis M, Piccini P, Pavese N, Koh SB, Brooks DJ. Evidence of dopamine dysfunction in the hypothalamus of patients with Parkinson's disease: An in vivo 11C-raclopride PET study. *Experimental Neurology*. 2008;214(1):112-116. doi:10.1016/j.expneurol.2008.07.021

30. Takashima H, Terada T, Bunai T, Matsudaira T, Obi T, Ouchi Y. In vivo Illustration of Altered Dopaminergic and GABAergic Systems in Early Parkinson's Disease. *Front Neurol*. 2022;13:880407. doi:10.3389/fneur.2022.880407

31. Yao NT, Zheng Q, Xu ZQ, et al. Positron emission computed tomography/single photon emission computed tomography in Parkinson disease. *Chinese Medical Journal*. 2020;133(12):1448-1455. doi:10.1097/CM9.0000000000000836

32. Huot P, Fox SH, Brotchie JM. The serotonergic system in Parkinson's disease. *Progress in Neurobiology*. 2011;95(2):163-212. doi:10.1016/j.pneurobio.2011.08.004

33. Melse M, Tan SKH, Temel Y, van Kroonenburgh MJPG, Leentjens AFG. Changes in 5-HT2A Receptor Expression in Untreated, de novo Patients with Parkinson's Disease. *Journal of Parkinson's Disease*. 2014;4(2):283-287. doi:10.3233/JPD-130300

34. Varrone A, Svenningsson P, Forsberg A, et al. Positron emission tomography imaging of 5-hydroxytryptamine1B receptors in Parkinson's disease. *Neurobiology of Aging*. 2014;35(4):867-875. doi:10.1016/j.neurobiolaging.2013.08.025

35. Kang Y, Henchcliffe C, Verma A, et al. 18F-FPEB PET/CT Shows mGluR5 Upregulation in Parkinson's Disease: mGluR5 and DaT in PD. *Journal of Neuroimaging*. 2019;29(1):97-103. doi:10.1111/jon.12563

36. Zhang Z, Zhang S, Fu P, et al. Roles of Glutamate Receptors in Parkinson's Disease. *IJMS*. 2019;20(18):4391. doi:10.3390/ijms20184391

37. Sharma A, Muresanu DF, Patnaik R, et al. Histamine H3 and H4 receptors modulate Parkinson's disease induced brain pathology. Neuroprotective effects of nanowired BF-2649 and clobenpropit with anti-histamine-antibody therapy. In: *Progress in Brain Research*. Vol 266. Elsevier; 2021:1-73. doi:10.1016/bs.pbr.2021.06.003

38. Meyer PM, Tiepolt S, Barthel H, Hesse S, Sabri O. Radioligand imaging of α4β2* nicotinic acetylcholine receptors in Alzheimer's disease and Parkinson's disease. *Q J Nucl Med Mol Imaging*. 2014;58(4):376-386.

39. Asahina M, Suhara T, Shinotoh H, Inoue O, Suzuki K, Hattori T. Brain muscarinic receptors in progressive supranuclear palsy and Parkinson's disease: a positron emission tomographic study. *Journal of Neurology, Neurosurgery & Psychiatry*. 1998;65(2):155-163. doi:10.1136/jnnp.65.2.155

40. van der Zee S, Kanel P, Gerritsen MJJ, et al. Altered Cholinergic Innervation in De Novo Parkinson's Disease with and Without Cognitive Impairment. *Movement Disorders*. 2022;37(4):713-723. doi:10.1002/mds.28913

41. Nahimi A, Kinnerup MB, Sommerauer M, Gjedde A, Borghammer P. Molecular Imaging of the Noradrenergic System in Idiopathic Parkinson's Disease. In: *International Review of Neurobiology*. Vol 141. Elsevier; 2018:251-274. doi:10.1016/bs.irn.2018.07.028

42. Brumberg J, Tran-Gia J, Lapa C, Isaias IU, Samnick S. PET imaging of noradrenaline transporters in Parkinson's disease: focus on scan time. *Ann Nucl Med*. 2019;33(2):69-77. doi:10.1007/s12149-018-1305-5

43. Smith SM, Alfaro-Almagro F, Miller KL. UK Biobank Brain Imaging Documentation (Version 1.8). Published online December 2020. Accessed February 13, 2023. https://biobank.ctsu.ox.ac.uk/crystal/crystal/docs/brain_mri.pdf

44. Friston KJ, Holmes AP, Worsley KJ, Poline JP, Frith CD, Frackowiak RSJ. Statistical parametric maps in functional imaging: A general linear approach. *Hum Brain Mapp*. 1994;2(4):189-210. doi:10.1002/hbm.460020402

45. Jenkinson M, Beckmann CF, Behrens TEJ, Woolrich MW, Smith SM. FSL. *NeuroImage*. 2012;62(2):782-790. doi:10.1016/j.neuroimage.2011.09.015

46. Whitfield-Gabrieli S, Nieto-Castanon A. Conn: A Functional Connectivity Toolbox for Correlated and Anticorrelated Brain Networks. *Brain Connectivity*. 2012;2(3):125-141. doi:10.1089/brain.2012.0073

47. Friston KJ, Williams S, Howard R, Frackowiak RSJ, Turner R. Movement-Related effects in fMRI time-series: Movement Artifacts in fMRI. *Magn Reson Med*. 1996;35(3):346-355. doi:10.1002/mrm.1910350312

48. Zou QH, Zhu CZ, Yang Y, et al. An improved approach to detection of amplitude of low-frequency fluctuation (ALFF) for resting-state fMRI: Fractional ALFF. *Journal of Neuroscience Methods*. 2008;172(1):137-141. doi:10.1016/j.jneumeth.2008.04.012

49. Deshpande G, LaConte S, Peltier S, Hu X. Integrated local correlation: A new measure of local coherence in fMRI data. *Hum Brain Mapp*. 2009;30(1):13-23. doi:10.1002/hbm.20482

50. Saad ZS, Reynolds RC, Jo HJ, et al. Correcting Brain-Wide Correlation Differences in Resting-State FMRI. *Brain Connectivity*. 2013;3(4):339-352. doi:10.1089/brain.2013.0156

51. Kasper J, Eickhoff SB, Caspers S, et al. Local synchronicity in dopamine-rich caudate nucleus influences Huntington's disease motor phenotype. *Brain*. Published online February 16, 2023:awad043. doi:10.1093/brain/awad043

52. Beliveau V, Ganz M, Feng L, et al. A High-Resolution *In Vivo* Atlas of the Human Brain's Serotonin System. *J Neurosci*. 2017;37(1):120-128. doi:10.1523/JNEUROSCI.2830-16.2016

53. Gallezot JD, Nabulsi N, Neumeister A, et al. Kinetic Modeling of the Serotonin 5-HT $_{1B}$ Receptor Radioligand [^{11} C]P943 in Humans. *J Cereb Blood Flow Metab*. 2010;30(1):196-210. doi:10.1038/jcbfm.2009.195

54. Kaller S, Rullmann M, Patt M, et al. Test–retest measurements of dopamine D1-type receptors using simultaneous PET/MRI imaging. *Eur J Nucl Med Mol Imaging*. 2017;44(6):1025-1032. doi:10.1007/s00259-017-3645-0

55. Sandiego CM, Gallezot JD, Lim K, et al. Reference Region Modeling Approaches for Amphetamine Challenge Studies with [^{11} C]FLB 457 and PET. *J Cereb Blood Flow Metab*. 2015;35(4):623-629. doi:10.1038/jcbfm.2014.237

56. Gallezot JD, Planeta B, Nabulsi N, et al. Determination of receptor occupancy in the presence of mass dose: [^{11} C]GSK189254 PET imaging of histamine H $_3$ receptor occupancy by PF-03654746. *J Cereb Blood Flow Metab*. 2017;37(3):1095-1107. doi:10.1177/0271678X16650697

57. Aghourian M, Legault-Denis C, Soucy JP, et al. Quantification of brain cholinergic denervation in Alzheimer's disease using PET imaging with [18F]-FEOBV. *Mol Psychiatry*. 2017;22(11):1531-1538. doi:10.1038/mp.2017.183

58. Naganawa M, Nabulsi N, Henry S, et al. First-in-Human Assessment of ^{11}C-LSN3172176, an M1 Muscarinic Acetylcholine Receptor PET Radiotracer. *J Nucl Med*. 2021;62(4):553-560. doi:10.2967/jnumed.120.246967

59. Hillmer AT, Esterlis I, Gallezot JD, et al. Imaging of cerebral α4β2* nicotinic acetylcholine receptors with (−)-[18F]Flubatine PET: Implementation of bolus plus constant infusion and sensitivity to acetylcholine in human brain. *NeuroImage*. 2016;141:71-80. doi:10.1016/j.neuroimage.2016.07.026

60. Smart K, Cox SML, Scala SG, et al. Sex differences in [11C]ABP688 binding: a positron emission tomography study of mGlu5 receptors. *Eur J Nucl Med Mol Imaging*. 2019;46(5):1179-1183. doi:10.1007/s00259-018-4252-4

61. Galovic M, Al-Diwani A, Vivekananda U, et al. In Vivo *NMDA Receptor Function in People with NMDA Receptor Antibody Encephalitis*. Neurology; 2021. doi:10.1101/2021.12.04.21267226

62. Normandin MD, Zheng MQ, Lin KS, et al. Imaging the Cannabinoid CB1 Receptor in Humans with [^{11}C] OMAR: Assessment of Kinetic Analysis Methods, Test–Retest Reproducibility, and Gender Differences. *J Cereb Blood Flow Metab*. 2015;35(8):1313-1322. doi:10.1038/jcbfm.2015.46

63. Bonett DG, Wright TA. Sample size requirements for estimating pearson, kendall and spearman correlations. *Psychometrika*. 2000;65(1):23-28. doi:10.1007/BF02294183

64. Rutherford S, Kia SM, Wolfers T, et al. The normative modeling framework for computational psychiatry. *Nat Protoc*. 2022;17(7):1711-1734. doi:10.1038/s41596-022-00696-5

65. Lotter LD, Saberi A, Hansen JY, et al. *Human Cortex Development Is Shaped by Molecular and Cellular Brain Systems*. Neuroscience; 2023. doi:10.1101/2023.05.05.539537

66. Vij SG, Nomi JS, Dajani DR, Uddin LQ. Evolution of spatial and temporal features of functional brain networks across the lifespan. *NeuroImage*. 2018;173:498-508. doi:10.1016/j.neuroimage.2018.02.066

67. Behfar Q, Behfar SK, Von Reutern B, et al. Graph Theory Analysis Reveals Resting-State Compensatory Mechanisms in Healthy Aging and Prodromal Alzheimer's Disease. *Front Aging Neurosci*. 2020;12:576627. doi:10.3389/fnagi.2020.576627

68. Humes LE, Busey TA, Craig J, Kewley-Port D. Are age-related changes in cognitive function driven by age-related changes in sensory processing? *Atten Percept Psychophys*. 2013;75(3):508-524. doi:10.3758/s13414-012-0406-9

69. Mozolic JL, Hugenschmidt CE, Peiffer AM, Laurienti PJ. Multisensory Integration and Aging. In: Murray MM, Wallace MT, eds. *The Neural Bases of Multisensory Processes*. Frontiers in Neuroscience. CRC Press/Taylor & Francis; 2012. Accessed September 18, 2023. http://www.ncbi.nlm.nih.gov/books/NBK92841/

70. Petitet P, Spitz G, Emir UE, Johansen-Berg H, O'Shea J. Age-related decline in cortical inhibitory tone strengthens motor memory. *NeuroImage*. 2021;245:118681. doi:10.1016/j.neuroimage.2021.118681

71. Bernier M, Croteau E, Castellano CA, Cunnane SC, Whittingstall K. Spatial distribution of resting-state BOLD regional homogeneity as a predictor of brain glucose uptake: A study in healthy aging. *NeuroImage*. 2017;150:14-22. doi:10.1016/j.neuroimage.2017.01.055

72. Oke AF, Carver LA, Gouvion CM, Adams RN. Three-dimensional mapping of norepinephrine and serotonin in human thalamus. *Brain Research*. 1997;763(1):69-78. doi:10.1016/S0006-8993(97)00404-6

73. Zitnik G, Chandler DJ, Waterhouse BD. Norepinephrine and Synaptic Transmission in the Cerebellum. In: Gruol DL, Koibuchi N, Manto M, Molinari M, Schmahmann JD, Shen Y, eds. *Essentials of Cerebellum and Cerebellar Disorders*. Springer International Publishing; 2016:237-241. doi:10.1007/978-3-319-24551-5_30

74. Cartford MC, Gould T, Bickford PC. A Central Role for Norepinephrine in the Modulation of Cerebellar Learning Tasks. *Behavioral and Cognitive Neuroscience Reviews*. 2004;3(2):131-138. doi:10.1177/1534582304270783

75. Bickford P. Aging and Motor Learning: A Possible Role for Norepinephrine in Cerebellar Plasticity. *Reviews in the Neurosciences*. 1995;6(1). doi:10.1515/REVNEURO.1995.6.1.35

76. Mather M. Noradrenaline in the aging brain: Promoting cognitive reserve or accelerating Alzheimer's disease? *Seminars in Cell & Developmental Biology*. 2021;116:108-124. doi:10.1016/j.semcdb.2021.05.013

77. Lee J, Kim HJ. Normal Aging Induces Changes in the Brain and Neurodegeneration Progress: Review of the Structural, Biochemical, Metabolic, Cellular, and Molecular Changes. *Front Aging Neurosci*. 2022;14:931536. doi:10.3389/fnagi.2022.931536

78. Guedj C, Monfardini E, Reynaud AJ, Farnè A, Meunier M, Hadj-Bouziane F. Boosting Norepinephrine Transmission Triggers Flexible Reconfiguration of Brain Networks at Rest. *Cereb Cortex*. Published online September 6, 2016:cercor;bhw262v1. doi:10.1093/cercor/bhw262

79. Chételat G, La Joie R, Villain N, et al. Amyloid imaging in cognitively normal individuals, at-risk populations and preclinical Alzheimer's disease. *NeuroImage: Clinical*. 2013;2:356-365. doi:10.1016/j.nicl.2013.02.006

80. Markesbery WR, Jicha GA, Liu H, Schmitt FA. Lewy Body Pathology in Normal Elderly Subjects. *J Neuropathol Exp Neurol*. 2009;68(7):816-822. doi:10.1097/NEN.0b013e3181ac10a7

81. Błaszczyk JW. Parkinson's Disease and Neurodegeneration: GABA-Collapse Hypothesis. *Front Neurosci*. 2016;10. doi:10.3389/fnins.2016.00269

82. Kaur R, Mehan S, Singh S. Understanding multifactorial architecture of Parkinson's disease: pathophysiology to management. *Neurol Sci*. 2019;40(1):13-23. doi:10.1007/s10072-018-3585-x

83. Wang J, Wang F, Mai D, Qu S. Molecular Mechanisms of Glutamate Toxicity in Parkinson's Disease. *Front Neurosci*. 2020;14:585584. doi:10.3389/fnins.2020.585584

84. Arias de la Torre J, Vilagut G, Ronaldson A, et al. Prevalence and age patterns of depression in the United Kingdom. A population-based study. *Journal of Affective Disorders*. 2021;279:164-172. doi:10.1016/j.jad.2020.09.129

85. Fry A, Littlejohns TJ, Sudlow C, et al. Comparison of Sociodemographic and Health-Related Characteristics of UK Biobank Participants With Those of the General Population. *American Journal of Epidemiology*. 2017;186(9):1026-1034. doi:10.1093/aje/kwx246

86. Nikhra V. The Aging Brain: Recent Research and Concepts. *GGS*. 2017;1(3). doi:10.31031/GGS.2017.01.000511

Tables:

	Healthy controls (HC)	*Females (HC)*	*Males (HC)*	**Manifest Parkinson's disease (PD)**	**HC matched to PD**
Sample Size	25 917	14 000	11 917	58	17400
Age [yr]	64.03 ± 7.5	63.5 ± 7.4	64.7 ± 7.6	68.6 ± 6.5	67.6 ± 6.0
Statistics		T = -12.48; P<0.0001; Cohen's d=-0.16		T(57.32)=1.15; P=0.26	
Sex	11917 (46.0%) M	-		32 (55.17%) M	8988 (51.7%) M
Statistics	-	-		χ2(1)=0.29, *P*=0.59	
TIV [L]	1.548 ± 0.152	1.467 ± 0.116	1.643 ± 0.133	-	-
Statistics	-	T = -113.0; P<0.0001; Cohen's d=-1.42		-	-

Table 1: Demographical characteristics. Normative modeling of co-localizations between brain function and neurotransmitter systems is based on the data of healthy controls. Regional differences in brain measures in patients with PD were calculated with respect to an age- and sex-matched subcohort of healthy controls.
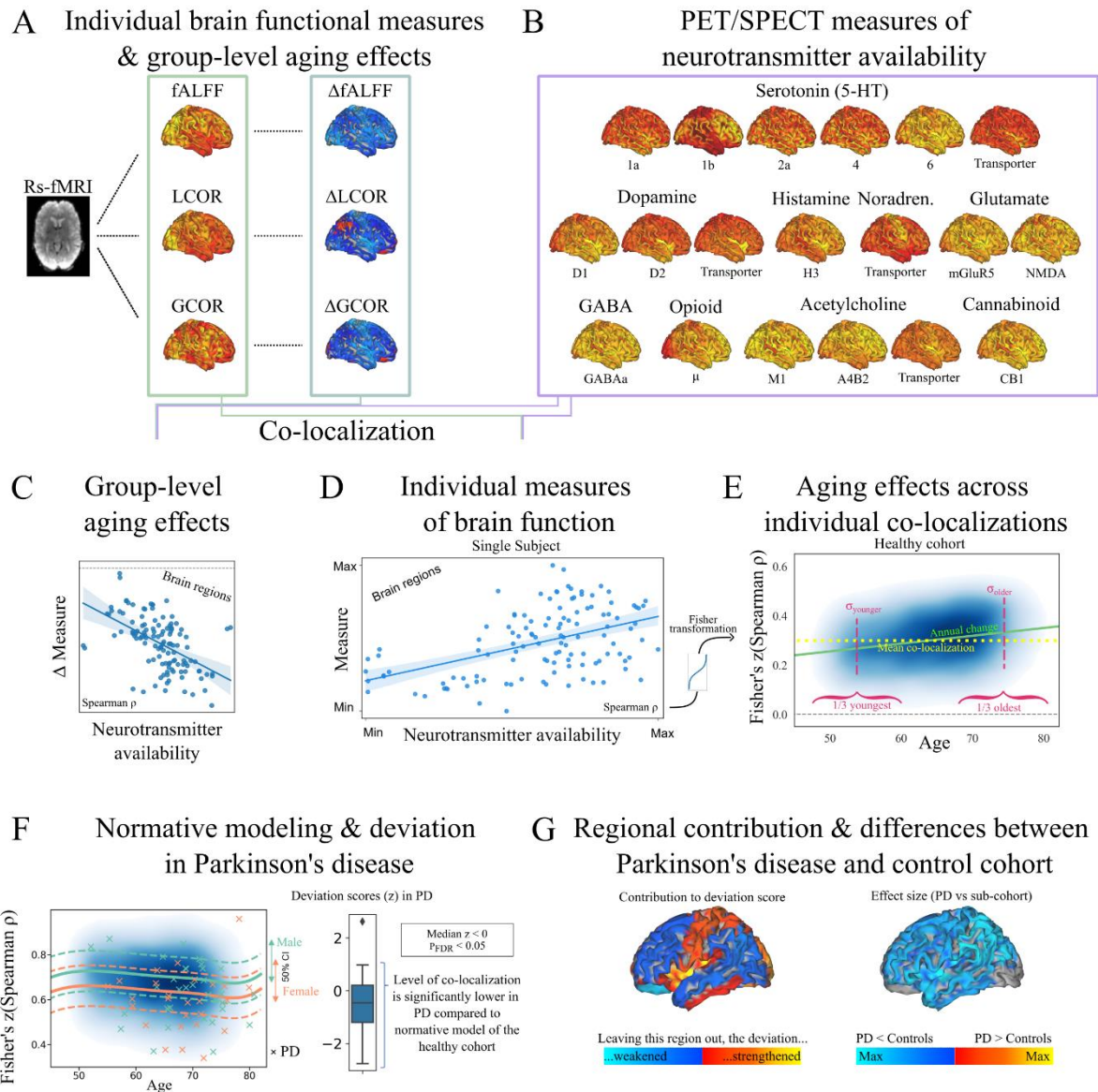
Figures:

Figure 1: Methodological overview. We derived voxel-wise maps of fALFF, LCOR, and GCOR from individual rs-fMRI data (**A**). First, this data was used to explore group-level voxel-wise aging changes in fALFF, LCOR and GCOR in the healthy cohort (n_{HC}=25,917, **A**, right column). Second, we used PET maps of 19 neurotransmitter systems (**B**) to calculate the spatial correlation (co-localization) with both, the group-level aging effects (**C**) and individual fALFF, LCOR, and GCOR (**D**). We Fisher (z-)transformed the Spearman correlation coefficients ρ to ensure a normal distribution and examined the effects of age on the co-localization data of the healthy cohort (**E**). The blue cloud illustrates co-localization strengths (kernel density estimation of all transformed Spearman correlation coefficients) of the healthy cohort. For each pair of measure and neurotransmitter map, we analyzed mean co-localizations (yellow), linear aging effects (green), as well as differences in variances across subjects in the youngest (44 - 60 years) and oldest (68 – 82 years) third (n_{Both} = 8,639; red). Vertical dashed red lines were added for illustration only and do not correspond to the actual variance of the respective subpopulation. Afterwards, we normatively modeled the co-localization strengths depending on age and sex (**F**, left) in order to calculate the deviation in subjects with manifest Parkinson's disease (n_{PD}=58; crosses). Here, we show the predicted means (solid lines) and 25% and 75% percentile (dashed lines) derived from the normative model for both men (blue) and women (orange). We analyzed whether the deviation (z-)scores of subjects with Parkinson's disease were significantly different from a null distribution (**F**, box plot). In this example, the distribution was significantly below a null distribution, indicating that patients with PD exhibit lower Spearman correlation coefficients than the norm. Last, we quantified the mean regional contribution to the observed deviation score across subjects with Parkinson's disease (**G**, left), as well as the functional differences in patients with Parkinson's disease compared to an age- and sex-matched subcohort of healthy controls ($n_{HCmatched}$ = 17,900; **G**, right). The functional differences were quantified by calculating the regional effect sizes (Cohen's d).
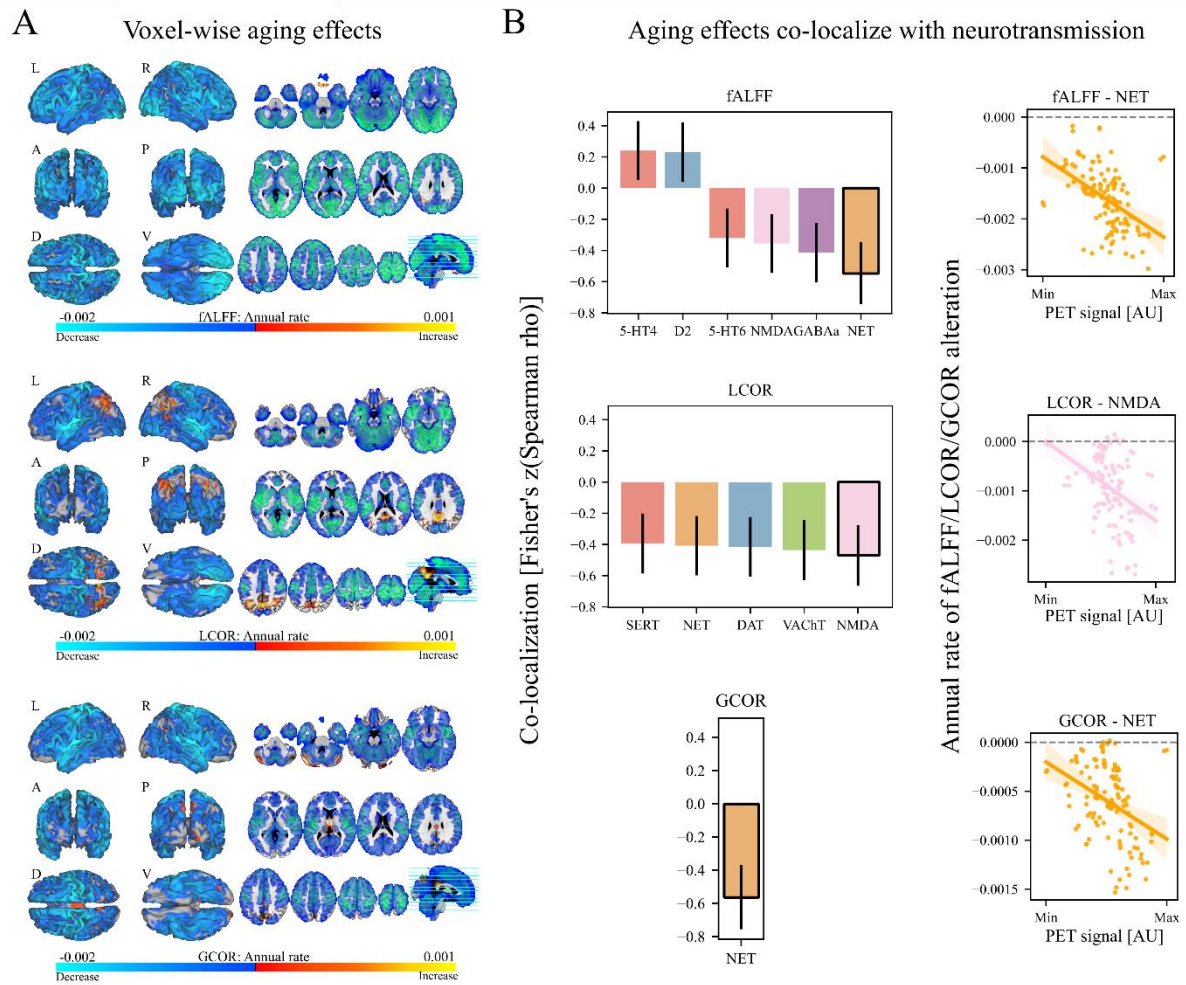
Figure 2: Group-level voxel-wise aging effects in each functional measure and associations with neurotransmitter systems. **A**: Colors in the voxel-wise plots of thresholded group-level aging effects indicate annual decrease (blue) or increase (red) in fALFF (top), LCOR (middle), and GCOR (bottom). **B, left column:** Significant (P_{FDR}< 0.05) linear correlations between annual rate in brain functional measure and neurotransmission. Vertical black lines indicate the uncertainty of Fisher's z-transformed Spearman correlation coefficient estimated according to Bonett & Wright[63]. **B, right column:** Exemplary scatter plots show how the annual change in fALFF, LCOR, or GCOR spatially correlate with the PET signal of specific neurotransmitter systems. Colors group receptors and transporters of the same neurotransmitter system, i.e., serotonin (red), dopamine (blue), acetylcholine (green), glutamate (pink) and GABA (purple), cannabinoid (mint), opioid (yellow), norepinephrine (orange), and histamine (turquoise).

Figure 3: Single-subject co-localizations between brain functional measure and neurotransmitter systems depend on age. **A, left column:** Overview about all significant linear aging effects ($P_{\text{Bonferroni-Holm}}<0.0001$) in the co-localization strengths (Fisher's z-transformed Spearman correlation coefficients) between each pair of brain functional measure (fALFF, LCOR, GCOR) and neurotransmitter system. Error bars correspond to the standard error of parameter (slope) estimation. **A, right column:** Exemplary plots show how co-localization strengths between brain functional measures (fALFF: top, LCOR: middle, GCOR: bottom) and specific neurotransmitter systems depend on age. The black, horizontal line indicate the population mean co-localization (cf. Supplemd Spentary Figure 6 for an overview abo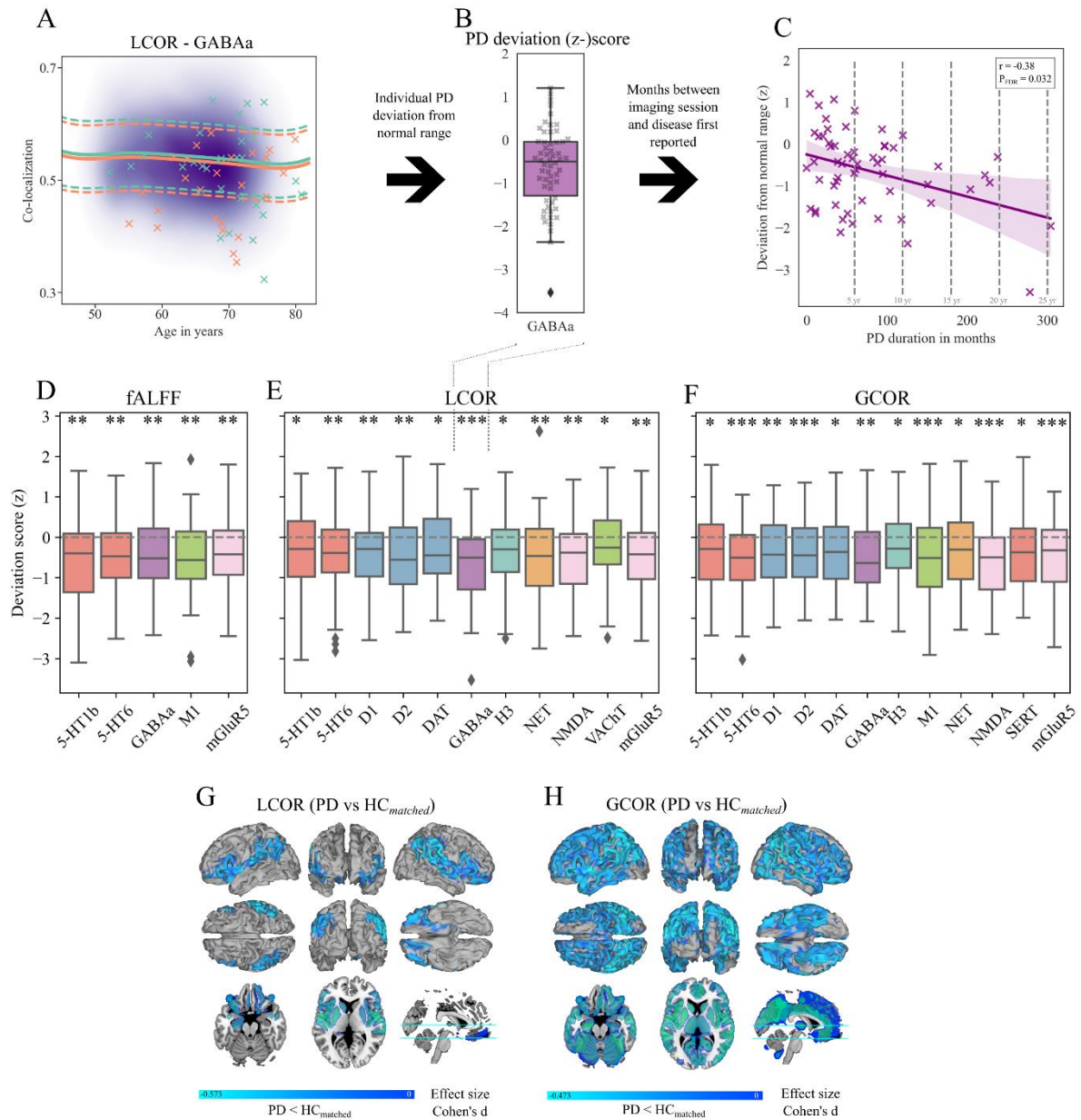ut all co-localization means). The colored clouds show the kernel density estimation of Fisher's z-transformed Spearman correlation coefficients of the healthy cohort. The slope of the colored line (linear fits) corresponds to the bar plots in the left column. **B, left column:** Each plot shows the effect size (F-statistic) of mean squared error (MSE) differences between younger and older adults. We show bar plots regarding neurotransmitter systems whose co-localization with the respective brain functional measure was previously shown to be significantly non-constant (White-test, $P_{\text{FDR}}<0.05$). All pairs of brain function and PET map whose co-localization variance was significantly ($P_{\text{FDR}}<0.05$) different between the older and the younger subpopulations are highlighted by asterisks (*: $P_{\text{FDR}}<0.05$; **: $P_{\text{FDR}}<0.01$; ***: $P_{\text{FDR}}<0.001$). F-statistics (MSE of older divided by MSE of younger adults) above 1 correspond to a larger variance in the older subpopulation. **B, right column:** Exemplary plots visualize the individual squared errors of the co-localizations between younger and older adults. Box plots visualize both distributions. Note, that per definition, the squared errors are positive. Due to the kernel density estimation of all squared errors the colored clouds exceed the null level. Colors group receptors and transporters of the same neurotransmitter system according to the same scheme as described in Figure 2.

Figure 4: Subjects with PD deviate from normative models of co-localization between brain function and neurotransmitter systems. **A**: The purple cloud shows the kernel-density-plot of Fisher's z-transformed Spearman correlation coefficients of the healthy cohort regarding the spatial correlation of LCOR and GABAa. Solid and dashed lines show the predicted mean and predicted 25% or 75% percentile of men (turquoise) and women (orange) derived from the normative models. Crosses indicate the co-localization levels of patients with PD. **B**: Box plot showing the significant deviation from the norm (null) in patients with PD. **C**: Deviation scores in PD are significantly correlated with disease duration. **D-F**: Box plots showing the deviation scores that were significantly different from the norm (null) regarding fALFF (**D**), LCOR (**E**), and GCOR (**F**). *, **, and *** indicate Bonferroni-Holm corrected significant deviations of the distributions from a null distribution with exact P<0.05, P<0.01, and P<0.001. Colors in box plots group receptors and transporters of the same neurotransmitter system according to the same scheme as described in Figure 2. **G-H:** Significant (P$_{FDR}$<0.05) regional differences (effect sizes, Cohen's d) between PD and the matched subgroup of healthy controls in LCOR (**G**) and GCOR (**H**). Lower values in PD are indicated by blue areas. Effect sizes of all region are provided in Supplementary Figures 17-19.